Available online at www.sciencedirect.com
ScienceDirect
Journal of the European Ceramic Society 27 (2007) 2957–2961
www.elsevier.com/locate/jeurceramsoc

The correlation between the structure and the dielectric properties of $K_xBa_{1-x}Ga_{2-x}Ge_{2+x}O_8$ ceramics

Marjeta Macek Krzmanc [a,*], Anton Meden [b], Danilo Suvorov [a]

[a] *Advanced Materials Department, Jožef Stefan Institute, Jamova 39, 1000 Ljubljana, Slovenia*
[b] *Faculty of Chemistry and Chemical Technology, University of Ljubljana, Aškerčeva 5, 1000 Ljubljana, Slovenia*

Available online 12 December 2006

Abstract

A study of $K_xBa_{1-x}Ga_{2-x}Ge_{2+x}O_8$ ceramics revealed that these solid solutions undergo a monoclinic-to-monoclinic $P2_1/a \Leftrightarrow C2/m$ phase transition. The temperature of this phase transition decreases with an increase in x, in a similar way to the sintering temperature, which decreases from 1100 °C ($x=0$) to 970 °C ($x=1$). The temperature of the $P2_1/a \Leftrightarrow C2/m$ phase transition is below the sintering temperatures of $K_xBa_{1-x}Ga_{2-x}Ge_{2+x}O_8$ ($0.67 \leq x \leq 1$) solid solutions, whereas the compositions at lower x ($x=0.4$ and 0) remain in the $P2_1/a$ modification over a wide temperature range above the sintering temperature. Compared to the $C2/m$ modification of $K_xBa_{1-x}Ga_{2-x}Ge_{2+x}O_8$ ($0.67 \leq x \leq 1$), with a permittivity of 6.2–6.9, the $P2_1/a$ modifications exhibit permittivities of 5.9–7.0 and three-to-eight times higher $Q \times f$ values of ~100,000 GHz (at ~12 GHz). The temperature coefficient of the resonant frequency is ~−25 ppm/K, regardless of the composition.

Keywords: Powders; X-ray methods; Dielectric properties

1. Introduction

The continuing growth in mobile telecommunications has increased the need for new, low-permittivity, low-loss materials. Firstly, due to their potential use as a substrate material, and secondly, due to the expansion of the utilized frequency range from the microwave (MW) to the millimetre-wave region. Low-temperature cofired ceramic (LTCC) technology imposes the additional requirement of a low sintering temperature: lower than 960 °C. The low sintering temperature of LTCC substrate materials can be achieved by recrystallization or by the addition of low-melting-point glass. Due to the presence of a glassy phase in both cases the dielectric losses are higher than in glass-free material.[1] However, this is to be expected, since the dielectric losses strongly depend on the structural order. The influence of ordering on Q-factor improvement in the perovskite-type $Ba(Zn_{1/3}Ta_{2/3})O_3$ has been the subject of many studies.[2] In contrast, the correlations between structural order and dielectric properties in feldspars are not so well investigated, even though the commercially used dielectrics for LTCC systems are based on the feldspar $MAl_2Si_2O_8$ (M = Ca, Sr, Ba) In our previous studies we attempted to determine some of these correlations for $Na_xCa_{1-x}Al_{2-x}Si_{2+x}O_8$ and $Sr_xBa_{1-x}Al_2Si_2O_8$ ceramics.[3,4] In an analogy with the solid solubility of $Na_xCa_{1-x}Al_{2-x}Si_{2+x}O_8$ we expected the existence of a solid solubility ($K_xBa_{1-x}Ga_{2-x}Ge_{2+x}O_8$) between $KGaGe_3O_8$ and $BaGa_2Ge_2O_8$, which has been reported to crystallize in the monoclinic paracelsian structure type with the space group $P2_1/a$.[5,6] The Ga- and Ge-containing feldspars could be interesting from the point of view of LTCC technology because of their sintering temperatures, which would be expected to be lower than the sintering temperature of aluminosilicate feldspars. In addition to this, the tetrahedral ordering, which strongly influences the dielectric losses in the MW frequency range, is known to be faster in Ge-containing feldspars.[7] These are the starting points for the synthesis and dielectric characterization of $K_xBa_{1-x}Ga_{2-x}Ge_{2+x}O_8$ solid solutions, the existence of which has not been reported yet. Our main focus was to study the $P2_1/a \Leftrightarrow C2/m$ phase transitions along the $K_xBa_{1-x}Ga_{2-x}Ge_{2+x}O_8$ solid-solubility range and correlate them with the dielectric properties.

2. Experimental

The $K_xBa_{1-x}Ga_{2-x}Ge_{2+x}O_8$ ($0 \leq x \leq 1$) solid solutions were synthesized using the solid-state reaction technique. Stoichiometric mixtures of reagent-grade oxides (Ga_2O_3, 99.99%,

* Corresponding author. Tel.: +386 1 477 3292; fax: +386 1 477 3875.
E-mail address: Marjeta.Macek@ijs.si (M. Macek Krzmanc).

0955-2219/$ – see front matter © 2006 Elsevier Ltd. All rights reserved.
doi:10.1016/j.jeurceramsoc.2006.11.021

Table 1
Pre-reaction, sintering and *C*2/*m* to $P2_1/a$ transformation conditions for $K_xBa_{1-x}Ga_{2-x}Ge_{2+x}O_8$ solid solutions ($0 \le x \le 1$)

Composition	Pre-reaction temperatures (°C)	Sintering temperature (°C), S.G.	Temperature for *C*2/*m* to $P2_1/a$ transformation (°C)
$KGaGe_3O_8$	600, 700, 800, 900, 930	970, *C*2/*m*	840
$K_{0.9}Ba_{0.1}Ga_{1.1}Ge_{2.9}O_8$	700, 800, 900, 970	990, *C*2/*m*	850
$K_{0.67}Ba_{0.33}Ga_{1.33}Ge_{2.67}O_8$	700, 800, 900, 1000	1020, *C*2/*m*	900
$K_{0.4}Ba_{0.6}Ga_{1.6}Ge_{2.4}O_8$	800, 900, 1000	1040, $P2_1/a$	–
$BaGa_2Ge_2O_8$	900, 1000	1100, $P2_1/a$	–

Aldrich, GeO_2, 99.999%, Alfa Aesar, K_2CO_3, 99.0%, Alfa Aesar and $BaCO_3$, 99.8% Alfa Aesar) were homogenized and pre-reacted under the conditions that are described in Table 1. Prior to sintering at 970–1100 °C the powders were milled with Y-stabilized ZrO_2 milling balls to a median particle size of 0.8 μm and isostatically pressed into pellets at ~130 MPa. In order to prepare $P2_1/a$ $K_xBa_{1-x}Ga_{2-x}Ge_{2+x}O_8$ ($0.67 \le x \le 1$) solid solutions the sintered ceramics were heat treated at $T \le 900$ °C (Table 1).

The X-ray powder-diffraction data were collected with a Bruker AXS D4 Endeavor diffractometer using Cu Kα radiation. The data were collected within the range $5° < 2\Theta < 90°$ with a step of 0.02°, a counting time of 10 s, and a variable V12 divergence slit. The Rietveld refinement TOPAS R program was used for the determination of the lattice parameters of the $K_xBa_{1-x}Ga_{2-x}Ge_{2+x}O_8$ ($0 \le x \le 1$) solid solutions with Rietveld refinement of the X-ray powder-diffraction data. All the structural parameters, except the unit-cell parameters, were kept fixed.

The microstructural studies of the samples were conducted with a scanning electron microscope (SEM) (Model JXA 840A, JEOL, Tokyo, Japan) coupled with energy-dispersive X-ray spectroscopy (EDX) and appropriate software (Series II X-ray microanalyzer, Tracor Nothern, Middleton, WI).

The radio-frequency (rf) dielectric measurements were performed at 1 MHz on In/Ga-plated disk capacitors using a high-precision LCR meter (Agilent 4284 A). The MW dielectric properties were characterized using the $TE_{01\delta}$ mode dielectric resonator method, developed by Krupka et al.[8] and a network analyzer (HP 8719C). The permittivity and dielectric loss tangent ($\tan\delta$) values were calculated at the resonant conditions ($TE_{01\delta}$ mode). Q values were calculated from the $\tan\delta$ values according to the equation $Q = 1/\tan\delta$. To determine the temperature coefficient of resonant frequency (τ_f) the test cavities were inserted into a temperature-controlled chamber. The dielectric characteristics of the samples were analyzed in the temperature range from 20 to 60 °C.

3. Results and discussion

3.1. Synthesis and crystallographic considerations for $K_xBa_{1-x}Ga_{2-x}Ge_{2+x}O_8$ ceramics

3.1.1. $K_xBa_{1-x}Ga_{2-x}Ge_{2+x}O_8$ (x = 1, 0.9 and 0.67)

The progress of the synthesis after each pre-reaction step was checked using the X-ray powder-diffraction technique. Due to the formation of several potassium–germanium and potassium-gallium oxide phases, whose diffraction lines overlapped, the X-ray diffraction patterns of the powders heat treated at $T < 900$ °C gave us little information about the reaction mechanism of the formation of $K_xBa_{1-x}Ga_{2-x}Ge_{2+x}O_8$ ($0.67 \le x \le 1$) solid solutions. The diffraction lines that did not correspond to any known structures of K-, Ba-, Ga- and Ge-containing compounds, additionally hindered the identification of the phases. When the pre-reaction temperature was increased to 900–1000 °C the XRD patterns of all three nominal compositions $K_xBa_{1-x}Ga_{2-x}Ge_{2+x}O_8$ ($x = 1$, 0.9 and 0.67) became very similar and did not change when the temperature was increased to higher temperatures below the melting point. Only a slight shift in the position of the diffraction lines was observed with the variation of x. This indicated the formation of solid solutions, which was additionally confirmed by the SEM investigations (Fig. 1). The monoclinic structure with the space group $P2_1/a$ is the only known structure of $KGaGe_3O_8$. However, the XRD pattern of the single-phase sample with the nominal composition $KGaGe_3O_8$ did not correspond to this structure. We found that the positions of the diffraction lines in this XRD pattern coincided with the diffraction lines of $KFeGe_3O_8$ with a monoclinic structure and the space group *C*2/*m*. Because of that the structure of the synthesized $KGaGe_3O_8$ was fitted (using Rietveld refinement) to determine the unit-cell parameters on the basis of the sanidine feldspar analogue (ICSD 59390),[9] modified to take into account the composition $KGaGe_3O_8$ instead of $KFeGe_3O_8$. The calculated pattern corresponded well to the experimental one (Fig. 2a). The structure of the synthesized $K_xBa_{1-x}Ga_{2-x}Ge_{2+x}O_8$ ($x = 0.9$, 0.67) was fitted in a similar way, taking into account the different composition (Fig. 2b). The unit-cell volumes obtained with the Rietveld structural refinement of the *C*2/*m* $K_xBa_{1-x}Ga_{2-x}Ge_{2+x}O_8$ ($x = 1, 0.9, 0.67$) powder data did not change significantly with composition in the range $0.67 \le x \le 1$ (Table 2).

The feldspars are known to exhibit an $I2/c \rightarrow C2/m$ order–disorder phase transition, where the *C*2/*m* structure is regarded as a disordered structure. This kind of phase transition was observed for the $BaAl_2Ge_2O_8$ feldspar, where the ordered (*I*2/*c*) structure was obtained by annealing at a temperature that was 400–500 °C below the temperature of the order–disorder phase transition.[7] Taking into account the fact that the *C*2/*m* structure was stable up to the melting point, we assumed that the known $P2_1/a$ (paracelsian) structure of $KGaGe_3O_8$ could be obtained by heat treating the *C*2/*m* structure at a temperature below the formation temperature of $KGaGe_3O_8$ (900 °C). The annealing of $K_xBa_{1-x}Ga_{2-x}Ge_{2+x}O_8$ ($x = 1$, 0.9, 0.67) in the temperature range 800–900 °C revealed that only at $x = 0.67$

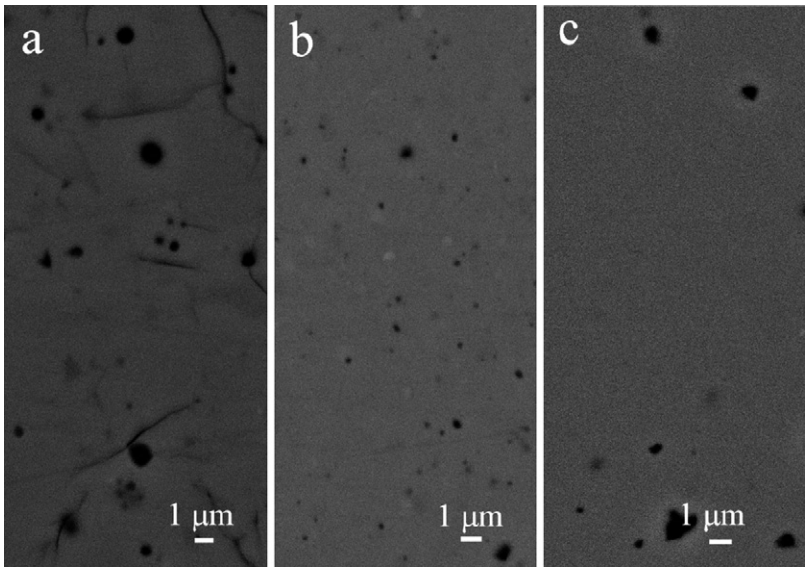

Fig. 1. SEM micrographs of $K_{0.67}Ba_{0.33}Ga_{1.33}Ge_{2.67}O_8$ (a), $K_{0.4}Ba_{0.6}Ga_{1.6}Ge_{2.4}O_8$ (b) and $BaGa_2Ge_2O_8$ (c) sintered at 1020, 1040 and 1100 °C.

was the $P2_1/a$ structure formed by heat treatment at 900 °C without encountering any problems with repeatability. In contrast, the $P2_1/a$ structure of $K_xBa_{1-x}Ga_{2-x}Ge_{2+x}O_8$ ($x = 1$, 0.9) was obtained by prolonged heat treatment (over 100 h) on $P2_1/a$ substrates at 840 and 850 °C, respectively. In order to elucidate how the unit-cell parameters change during the $P2_1/a \Leftrightarrow C2/m$ phase transition a Rietveld refinement of the X-ray diffraction data was performed. The $P2_1/a$ structures of $K_xBa_{1-x}Ga_{2-x}Ge_{2+x}O_8$ ($x = 1$, 0.9, 0.67) were fitted on the basis of $KGaGe_3O_8$ (ICSD 1022)[9] crystal-structure data ($P2_1/a$) that were modified to take into account the composition (Fig. 3). The decrease in the unit-cell volume with the increase in Ba content was to be expected, based on literature where a larger unit-cell volume was reported for $KGaGe_3O_8$ (ICSD 1022)[9] than for $BaGa_2Ge_2O_8$ (ICSD 368)[9] (Table 2). If we compare the unit-cell volume of the $P2_1/a$ and $C2/m$ phases at various $K_xBa_{1-x}Ga_{2-x}Ge_{2+x}O_8$ compositions ($x = 1$, 0.9, 0.67) we find that the transition from the $C2/m$ phase to the $P2_1/a$ phase is accompanied by an increase in the unit-cell volume at $x = 1$ and 0.9 (Table 2). In contrast, there is only small difference in the unit-cell volumes of the $C2/m$ and $P2_1/a$ structures of $K_{0.67}Ba_{0.33}Ga_{1.33}Ge_{2.67}O_8$ ($x = 0.67$) (Table 2). This increase in the unit-cell volume was most probably the reason for the cracks that formed during the heat treatment of the $K_{0.9}Ba_{0.1}Ga_{1.1}Ge_{2.9}O_8$ and $KGaGe_3O_8$ resonators at 850 and 840 °C, respectively. The SEM micrographs revealed the single-phase structure with lines (Fig. 1a) that were only observed at compositions ($0.67 \leq x \leq 1$) that were sintered above $P2_1/a \Leftrightarrow C2/m$ phase transition.

3.1.2. $K_xBa_{1-x}Ga_{2-x}Ge_{2+x}O_8$ ($x = 0.4$ and 0)

The XRD analysis of the pre-reacted powders with the nominal compositions $K_{0.4}Ba_{0.6}Ga_{1.6}Ge_{2.4}O_8$ and $BaGa_2Ge_2O_8$ revealed that the paracelsian ($P2_1/a$) phase was already formed at 900 °C. Barium germanium and barium gallium oxides were also present in considerable quantities at this temperature. The paracelsian ($P2_1/a$) phase, which was completely formed at 1000 °C, was still preserved during the sintering of $K_{0.4}Ba_{0.6}Ga_{1.6}Ge_{2.4}O_8$ and $BaGa_2Ge_2O_8$ at 1040 and 1100 °C, respectively. The SEM micrographs of $K_{0.4}Ba_{0.6}Ga_{1.6}Ge_{2.4}O_8$ also revealed a single-phase structure without the lines, typ-

Table 2
Unit-cell parameters of $C2/m$ and $P2_1/a$ $K_xBa_{1-x}Ga_{2-x}Ge_{2+x}O_8$ solid solutions

Composition	Structure	Unit-cell parameters				
		a (Å)	b (Å)	c (Å)	β (°)	V (Å^3)
$KGaGe_3O_8$	$P2_1/a$	9.4906(4)	9.8915(3)	8.7210(3)	90.043(5)	818.69(5)
	$C2/m$	8.873(1)	13.636(2)	7.490(1)	115.945(9)	814.9(1)
$K_{0.9}Ba_{0.1}Ga_{1.1}Ge_{2.9}O_8$	$P2_1/a$	9.4667(4)	9.8927(4)	8.7305(4)	90.032(7)	817.63(6)
	$C2/m$	8.8639(9)	13.630(1)	7.4904(7)	115.738(6)	815.2(1)
$K_{0.67}Ba_{0.33}Ga_{1.33}Ge_{2.67}O_8$	$P2_1/a$	9.4251(4)	9.8912(4)	8.7480(4)	89.9(3)	815.54(6)
	$C2/m$	8.8550(6)	13.609(1)	7.4872(5)	115.402(4)	815.05(9)
$K_{0.4}Ba_{0.6}Ga_{1.6}Ge_{2.4}O_8$	$P2_1/a$	9.4001(6)	9.8863(6)	8.7693(6)	90.062(7)	814.95(9)
	$C2/m$	–	–	–	–	–
$BaGa_2Ge_2O_8$	$P2_1/a$	9.3558(7)	9.9099(8)	8.7855(7)	90.253(6)	814.5(1)
	$C2/m$	–	–	–	–	–

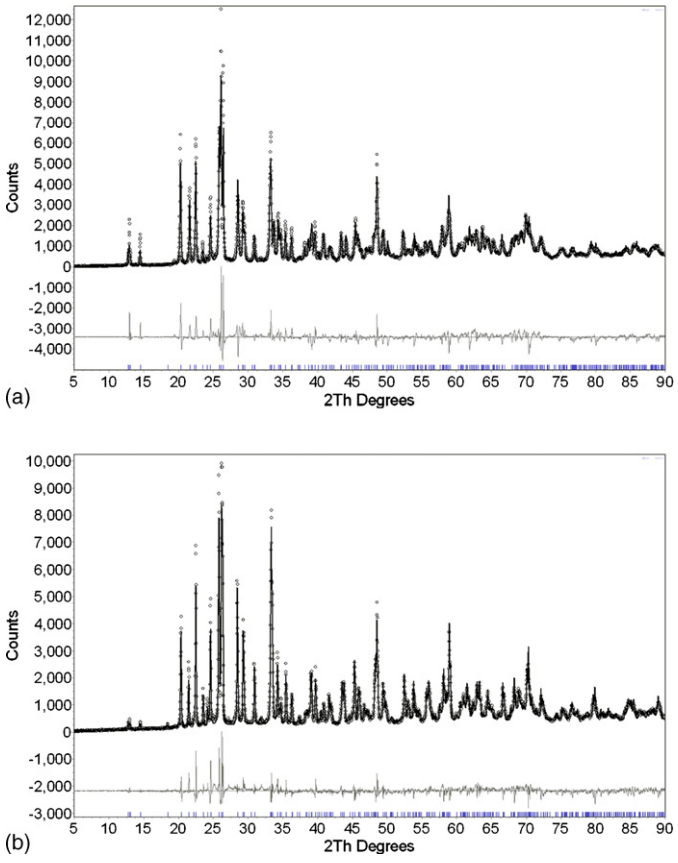

Fig. 2. Comparison between the calculated XRD patterns of $KGaGe_3O_8$ (a) and $K_{0.67}Ba_{0.33}Ga_{1.33}Ge_{2.67}O_8$ (b) obtained by Rietweld refinement on the basis of the modified sanidine feldspar analogue (S.G. *C*2/*m*) $KFeGe_3O_8$ structural data (ICSD 59390)[9] and the XRD pattern of $KGaGe_3O_8$ (a) and $K_{0.67}Ba_{0.33}Ga_{1.33}Ge_{2.67}O_8$ (b) powders. Calculated XRD pattern (—), experimental XRD pattern (○○○○), and difference curve (▬▬). Vertical bars denote reflection positions.

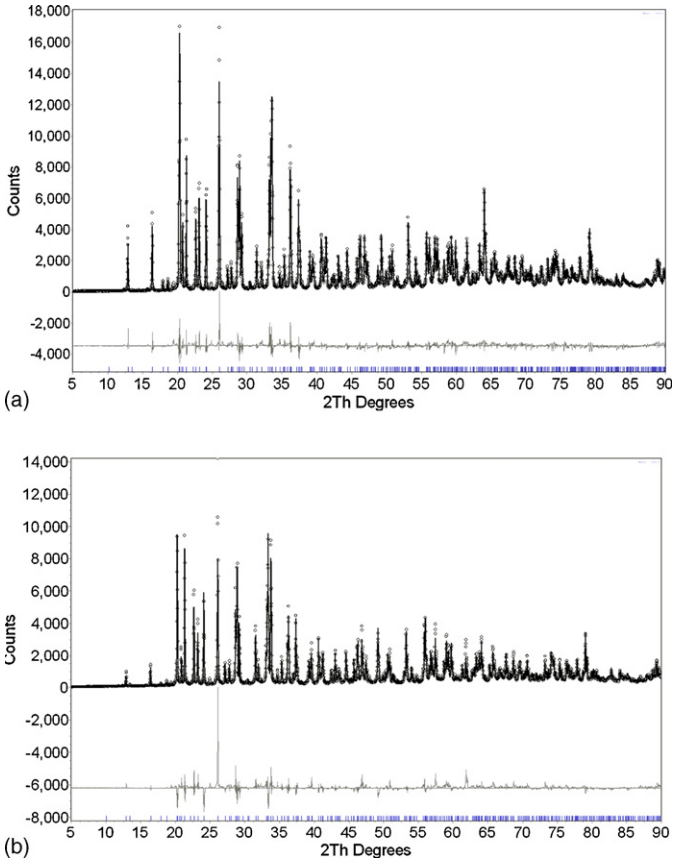

Fig. 3. Comparison between the calculated XRD patterns of $KGaGe_3O_8$ (a) and $K_{0.67}Ba_{0.33}Ga_{1.33}Ge_{2.67}O_8$ (b) obtained by Rietveld refinement on the basis of modified $KGaGe_3O_8$ (S.G. $P2_1/a$) structural data (ICSD 1022)[9] and the XRD pattern of $KGaGe_3O_8$ (a) and $K_{0.67}Ba_{0.33}Ga_{1.33}Ge_{2.67}O_8$ (b) powders, which were heat treated at 840 and 900 °C, respectively. Calculated XRD pattern (—), experimental XRD pattern (○○○○), and difference curve (▬▬). Vertical bars denote reflection positions.

ical of $K_xBa_{1-x}Ga_{2-x}Ge_{2+x}O_8$ ($0.67 \le x \le 1$) with the *C*2/*m* structure (Fig. 1). In analogy with the solid solutions at higher x ($0.67 \le x \le 1$) we expected that $K_{0.4}Ba_{0.6}Ga_{1.6}Ge_{2.4}O_8$ and $BaGa_2Ge_2O_8$ would also undergo the $P2_1/a \Leftrightarrow C2/m$ phase transition. The *C*2/*m* modification of $K_{0.4}Ba_{0.6}Ga_{1.6}Ge_{2.4}O_8$ was observed only at $T > 1130$ °C. In contrast, we observed no changes in the XRD pattern of $BaGa_2Ge_2O_8$, even after 36 h of heat treatment at 1250 °C (20–30 °C below the melting point). In order to obtain the unit-cell parameters of the $P2_1/a$ $K_{0.4}Ba_{0.6}Ga_{1.6}Ge_{2.4}O_8$ and $BaGa_2Ge_2O_8$ the structures were fitted on the basis of $BaGa_2Ge_2O_8$ (ICSD 368)[9] crystal-structure data ($P2_1/a$) that were modified to take into account the composition (Table 2).

3.2. Dielectric characterization

For the analysis of the dielectric properties the powders were sintered to dense ceramics with a relative density greater than 95%. A typical remaining level of porosity is shown in Fig. 1. If we compare the density of the $K_xBa_{1-x}Ga_{2-x}Ge_{2+x}O_8$ ceramics sintered above ($0.67 \le x \le 1$) and those ($x = 0.4$ and 0) sintered below the $P2_1/a \Leftrightarrow C2/m$ transition we see that the former were less dense (Fig. 1). Because of this, there is some extrinsic contribution to the measured dielectric properties (Table 3). Due to the higher porosity of the $K_xBa_{1-x}Ga_{2-x}Ge_{2+x}O_8$ ($0.67 \le x \le 1$) ceramics the experimentally determined permittivity can be lower than the theoretical one.

Only the $K_{0.67}Ba_{0.33}Ga_{1.33}Ge_{2.67}O_8$ ceramic was dielectrically characterized in both crystallographic forms. The cracks that formed in the $K_{0.9}Ba_{0.1}Ga_{1.1}Ge_{2.9}O_8$ and $KGaGe_3O_8$ resonators during the transformation from the *C*2/*m* to the $P2_1/a$ phase prevented their characterization in the MW frequency range. It is clear from Table 3 that the $P2_1/a$ modification of the $K_{0.67}Ba_{0.33}Ga_{1.33}Ge_{2.67}O_8$ ceramic exhibits a three-times-higher $Q \times f$ value and a lower permittivity than the *C*2/*m* modification. At the same time there is no significant change of τ_f. The *C*2/*m* modification of the $K_{0.9}Ba_{0.1}Ga_{1.1}Ge_{2.9}O_8$ and $KGaGe_3O_8$ ceramics exhibits even lower $Q \times f$ values than the *C*2/*m* modification of $K_{0.67}Ba_{0.33}Ga_{1.33}Ge_{2.67}O_8$. In contrast, the $Q \times f$ values of the $P2_1/a$ forms ($0 \le x \le 1$) were in the range 94,700–106,400 GHz (Table 3). The resonators and capacitors of the *C*2/*m* $K_{0.4}Ba_{0.6}Ga_{1.6}Ge_{2.4}O_8$ were not prepared and dielectrically characterized due to the evaporation of potassium that can occur at the temperature of the $P2_1/a \Leftrightarrow C2/m$ transformation (1130 °C).

Table 3
The dielectric properties of $K_xBa_{1-x}Ga_{2-x}Ge_{2+x}O_8$ ($0 \le x \le 1$) solid solutions determined at 1 MHz and in the microwave frequency region (at ~12 GHz)

Composition	Structure	rf	MW		
		ε	ε	$Q \times f$ (GHz)	τ_f (ppm/K)
$KGaGe_3O_8$	$P2_1/a$	–	–	–	–
	$C2/m$	6.4	6.2	19,800	−21
$K_{0.9}Ba_{0.1}Ga_{1.1}Ge_{2.9}O_8$	$P2_1/a$	–	–	–	–
	$C2/m$	7.5	6.6	12,680	−21
$K_{0.67}Ba_{0.33}Ga_{1.33}Ge_{2.67}O_8$	$P2_1/a$	5.8	5.9	94,100	−25
	$C2/m$	6.9	6.9	32,660	−27
$K_{0.4}Ba_{0.6}Ga_{1.6}Ge_{2.4}O_8$	$P2_1/a$	6.5	6.4	94,700	−23
	$C2/m$	–	–	–	–
$BaGa_2Ge_2O_8$	$P2_1/a$	7.1	7.0	106,400	−25
	$C2/m$	–	–	–	–

Since the microwave dielectric measurements revealed that the $Q \times f$ values decreased during the $P2_1/a \Leftrightarrow C2/m$ transformation, we tried to follow this transformation in $BaGa_2Ge_2O_8$ by measuring the microwave dielectric losses. The $Q \times f$ values of $BaGa_2Ge_2O_8$ slowly decrease with the prolongation of the heat-treatment time at 1250 °C. After 36 h of such a heat treatment the $Q \times f$ values were lower by ~30%. In spite of this relatively big difference in dielectric losses, no difference in the XRD patterns was observed.

On the basis of measurements of the microwave dielectric losses, which are sensitive to the structural order, we can assume that the $P2_1/a$ structure is most probably more ordered than the $C2/m$ structure. However, this remains to be proved by a detailed crystallographic analysis.

4. Conclusions

$K_xBa_{1-x}Ga_{2-x}Ge_{2+x}O_8$ ceramics undergo a monoclinic–monoclinic $P2_1/a \Leftrightarrow C2/m$ phase transition. The temperature of this transition increases with a decrease in x. The $C2/m$ form was obtained during the synthesis and sintering of $K_xBa_{1-x}Ga_{2-x}Ge_{2+x}O_8$ ($0.67 \le x \le 1$), whereas $K_{0.4}Ba_{0.6}Ga_{1.6}Ge_{2.4}O_8$ ($x = 0.4$) and $BaGa_2Ge_2O_8$ ($x = 0$) remained in the $P2_1/a$ form over a wide temperature range above the sintering temperature. $KGaGe_3O_8$ and $K_{0.9}Ba_{0.1}Ga_{1.1}Ge_{2.9}O_8$ ceramics can be sintered at 970 and 990 °C, respectively. However, the relatively large increase in the unit-cell volume that occurred during the $C2/m$-to-$P2_1/a$ transformation prevented the dielectric characterization of the $P2_1/a$ modification of the $KGaGe_3O_8$ and $K_{0.9}Ba_{0.1}Ga_{1.1}Ge_{2.9}O_8$ ceramics. The $P2_1/a$ $K_xBa_{1-x}Ga_{2-x}Ge_{2+x}O_8$ ($0 \le x \le 0.67$) solid solutions exhibit a permittivity of 5.9–7.0, $Q \times f$ values of 95,000–106,000 GHz and a τ_f of ~−25 ppm/K.

Due to the low sintering temperature (1020–1100 °C) and their high $Q \times f$ values the $P2_1/a$ $K_xBa_{1-x}Ga_{2-x}Ge_{2+x}O_8$ ceramics are promising candidates for microwave applications and LTCC technology.

References

1. Valant, M. and Suvorov, D., Glass-free low-temperature cofired ceramics: calcium germanates, silicates and tellurates. *J. Eur. Ceram. Soc.*, 2004, **24**, 1715–1719.
2. Kog, E., Yamagishi, Y., Moriwake, H., Kakimoto, K. and Ohsato, H., Large Q factor variation within dense, highly ordered $Ba(Zn_{1/3}Ta_{2/3})O_3$ system. *J. Eur. Ceram. Soc.*, 2006, **26**, 1961–1964.
3. Macek Krzmanc, M., Valant, M., Jancar, B. and Suvorov, D., Sub-solidus synthesis and microwave dielectric characterization of plagioclase feldspars. *J. Am. Ceram. Soc.*, 2005, **88**(9), 2472–2479.
4. Macek Krzmanc, M., Valant, M. and Suvorov, D., The synthesis and microwave dielectric properties of $Sr_xBa_{1-x}Al_2Si_2O_8$ and $Ca_yBa_{1-y}Al_2Si_2O_8$ ceramics. *J. Eur. Ceram. Soc.*, 2007, **27**(2–3), 1181–1185.
5. Klaska, R. and Jarchow, O., $KGaGe_3O_8$, ein Paracelsian-Typ mit einwertigen Kation. *Naturwissenschaften*, 1977, **64**, 92–93.
6. Calleri, M. and Gazzoni, G., The structures of (Sr, Ba)[(Al, Ga)2(Si, Ge)2O8]III. The crystal structures of the paracelsian like modifications of synthetic $SrGa_2Ge_2O_8$ and $BaGa_2Ge_2O_8$. *Acta Cryst.*, 1976, **B32**, 1196–1205.
7. Malcherek, T., Kroll, H., Schleiter, M. and Salje, E. K. H., The kinetics of the monoclinic to monoclinic phase transition in $BaAl_2Ge_2O_8$-feldspar. *Phase Transit.*, 1995, **55**, 199–215.
8. Krupka, J., Derzakowski, K., Riddle, B. and Baker-Jarvis, J., A dielectric resonator for measurements of complex permittivity of low loss dielectric materials as a function of temperature. *Meas. Sci. Technol.*, 1998, **9**, 1751–1756.
9. *FIZ/NIST Inorganic Crystal Structure Database Version 1.2.1., Faschinformations zentrum*, Karlsruhe, National Institute of Standards and Technology, July 2003.